IEEE Access
Multidisciplinary ⋮ Rapid Review ⋮ Open Access Journal

Received March 8, 2021, accepted April 3, 2021, date of publication April 13, 2021, date of current version April 27, 2021.

Digital Object Identifier 10.1109/ACCESS.2021.3072845

Demonstration of MOCVD-Grown Long-Wavelength Infrared InAs/GaSb Superlattice Focal Plane Array

YAN TENG[1,2], XIUJUN HAO[2,3], HONG ZHU[2,4], HE ZHU[1,2], JIAFENG LIU[1,2], YUNLONG HUAI[1,2], MENG LI[2,3], MING LIU[5], WEIRONG XING[5], BAILE CHEN[6], (Senior Member, IEEE), ZHUO DENG[6], AND YONG HUANG[1,2]

[1]School of Nano-Tech and Nano-Bionics, University of Science and Technology of China, Hefei 230026, China
[2]Key Laboratory of Nanodevices and Applications, Suzhou Institute of Nano-Tech and Nano-Bionics, Chinese Academy of Sciences (CAS), Suzhou 215123, China
[3]School of Physical Science and Technology, ShanghaiTech University, Shanghai 201210, China
[4]Nano Science and Technology Institute, University of Science and Technology of China, Hefei 230026, China
[5]North China Research Institute of Electro-Optics, Beijing 100015, China
[6]School of Information Science and Technology, ShanghaiTech University, Shanghai 201210, China

Corresponding author: Yong Huang (yhuang2014@sinano.ac.cn)

This work was supported by the National Natural Science Foundation of China under Grant 61874179, Grant 61804161, Grant 62074156, and Grant 61975121.

ABSTRACT High-performance InAs/GaSb type-II superlattice infrared detectors and focal plane arrays (FPAs) are normally grown by molecular beam epitaxy (MBE). In this work, we demonstrate the first long-wavelength infrared InAs/GaSb superlattice FPA grown by metalorganic chemical vapor deposition (MOCVD) with clear image. High-quality superlattice material was obtained evidenced by sharp X-ray diffraction peaks and atomic flat surface. Electrical and optical measurements performed on single element detectors showed a 50% cut-off wavelength of $\sim$10.1 μm, a dark current density of 2.5×10^{-5} A/cm^2, a peak responsivity of 0.88 A/W and a peak detectivity of 1.7×10^{11} cm·Hz$^{1/2}$/W at 80 K. A 320×256 FPA with 30 μm pixel pitch was then fabricated. With an integration time of 1.9 ms and an applied bias of -0.1 V, the FPA shows an average operability of 96.96%, a non-uniformity of 4.97%, a noise equivalent temperature difference of 51.1 mK and a peak detectivity of 2.3×10^{10} cm·Hz$^{1/2}$/W at 80 K without thinning down the substrate.

INDEX TERMS Long-wavelength infrared, InAs/GaSb superlattice, focal plane array, metalorganic chemical vapor deposition.

I. INTRODUCTION

Long-wavelength infrared (LWIR) focal plane arrays (FPAs) with 50% cut-off wavelength of 8 to 12 μm have broad applications in diagnosis assistance, industrial process monitoring, and night vision. Compared to the dominant HgCdTe technology used in LWIR detection, InAs/GaSb type-II superlattices (T2SLs) have the merits of low Auger recombination rate [1], good material uniformity [2] and low fabrication cost [3]. Up to now, all the InAs/GaSb T2SL FPAs have been exclusively grown by molecular beam epitaxy (MBE) [4]–[10]. On the other hand, metalorganic chemical vapor deposition (MOCVD), as the industry leading epitaxy technique, has the advantages of high throughput production, easy maintenance process, and flexible reactor configuration. Recently, Wu *et al*. reported MOCVD-grown LWIR InAs/InAsSb SL single element detectors with a peak detectivity of 5.4×10^{10} cm·Hz$^{1/2}$/W [11]. In our group, we have carried out extensively the growth of Sb-based materials by MOCVD [12], [13]. We previously reported high-quality InAs/GaSb SL materials grown by MOCVD with nearly zero strain and atomic flat surface by inserting GaAs-like interfacial layers [14]. Scanning transmission electron microscopy (STEM) also reveals very abrupt interfaces with narrow interface widths in MOCVD-grown T2SLs [15]. Recently, we have proposed and demonstrated

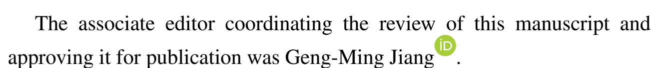
The associate editor coordinating the review of this manuscript and approving it for publication was Geng-Ming Jiang.

This work is licensed under a Creative Commons Attribution 4.0 License. For more information, see https://creativecommons.org/licenses/by/4.0/

high-performance LWIR detectors with Al-free single heterojunction structure named "PNn" [16], [17].

In the PNn structure, the space charge region is only confined in the mid-wavelength barrier layer and LWIR absorber remains a flat band condition., which reduces the generation-recombination (G-R) and tunneling current. In addition, this structure can also be exploited to realize bias-selectable dual-band detection [18]. We have achieved LWIR PNn detectors with the peak detectivity of 7.3 × 10^{11} cm·Hz$^{1/2}$/W and 1.0 × 10^{11} cm·Hz$^{1/2}$/W at the cut-off wavelength of 8 and 12 μm, respectively [16], [17]. In this paper, we demonstrate a MOCVD-grown LWIR T2SL single detector and FPA at a cut-off wavelength of around 10 μm. To the best of our knowledge, this is the first antimonide-based LWIR FPA demonstrated by MOCVD.

II. MATERIALS GROWTH AND CHARACTERIZATION

The detector structure was grown on a 2-inch InAs (100) wafer using an Aixtron MOCVD reactor. More details about the growth conditions, growth uniformity evaluation and photodiode structure can be found elsewhere [14], [16], [17]. The detector structure was started with a 0.5 μm thick Si-doped n-type (2.0 × 10^{18} cm^{-3}) InAs contact layer and a 2.0 μm thick Si-doped n-type (2.0 × 10^{16} cm^{-3}) long-wavelength SL (LWSL) absorber layer. Then, a 110 nm thick Si-doped n-type (2.0 × 10^{16} cm^{-3}) mid-wavelength SL (MWSL) electron-barrier layer was grown followed by a 500 nm thick Zn-doped p-type (1 × 10^{18} cm^{-3}) MWSL contact layer. Finally, the whole structure was capped with a 20 nm thick Zn-doped p-type (1 × 10^{18} cm^{-3}) GaSb layer. The LWSL was designed to have a cutoff-wavelength of 10 μm with 20/8 monolayers (MLs) of InAs/GaSb, whereas 6/8 MLs of InAs/GaSb is chosen for the MWSL with an estimated effective bandgap of 0.3 eV. X-ray diffraction (XRD) and atomic force microscopy (AFM) were used as the material characterization tools. For structural evaluation, the XRD curve in ω-2θ scan mode and corresponding simulation curve of the epitaxial structure along the InAs (004) direction were presented in Fig. 1(a). The full-width at half maximum (FWHM) of the ±1st order peak for the LWSL absorber is as low as 38 arcsec. Up to ±4th order satellite peaks for LWSLs are visible. These sharp satellite peaks and high order diffraction indicate excellent periodicity and crystalline quality of the epitaxial structure. For surface characterization, the surface morphology measured by AFM is shown in Fig. 1(b). The sample exhibits a smooth surface with a root mean square (RMS) roughness of only 0.206 nm over a 5 × 5 μm^2 scan area. Both XRD and AFM characterization indicate the high crystalline quality of the MOCVD-grown epitaxial materials. Single element detectors and FPAs are fabricated from this epitaxial material.

III. MOCVD-GROWN InAs/GaSb SUPERLATTICE SINGLE ELEMENT DETECTORS

For single element detector fabrication, diodes with sizes ranging from 150 × 150 to 800 × 800 μm^2 were processed by standard lithography and inductively coupled plasma (ICP) dry etching. A 200 nm thick SiO_2 passivation layer was deposited by plasma enhanced chemical vapor deposition (PECVD). Then reactive ion etching (RIE) was used to for window opening. Finally, top and bottom metals of the diodes were formed by depositing Ti (25 nm)/Pt (55 nm)/Au (300 nm). No antireflection coating was applied.

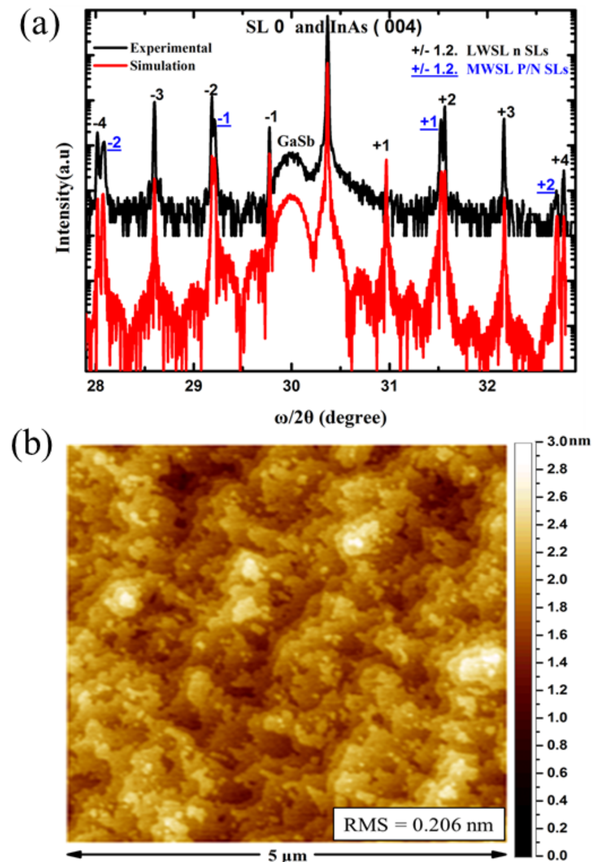

FIGURE 1. (a) XRD ω-2θ curve and corresponding simulation curve of the epitaxial structure along the InAs (004) direction. (b) AFM image of epitaxial material.

The dark current measurement of single element detector was performed at 80 K. Fig. 2(a) shows the current–voltage characteristics and corresponding differential resistance area product (RA) of the diodes. At -0.1 V, dark current density (J_d) and RA are determined as 2.5 × 10^{-5} A/cm^2 and 2871.8 Ω·cm^2, respectively. RA at zero bias (R_0A) is up to 1348.6 Ω·cm^2. The inset of Fig. 2(a) shows the measured J_d as a function of the perimeter to area ratio. The surface resistivity ($r_{surface}$) is calculated using the following equation:

$$J_d = (J_{bulk} + \frac{V_b}{r_{surface}} \times P/A) \quad (1)$$

In Eq. (1), J_{bulk}, V_b, P, and A correspond to the bulk current contribution, the applied bias voltage, the perimeter and the area, respectively. The $r_{surface}$ is calculated to be 2.2 × 10^5Ω·cm, which is close to the reported results for infrared detectors with the optimized process [19], [20]. Then, the spectral response (R_λ) of a single element detector

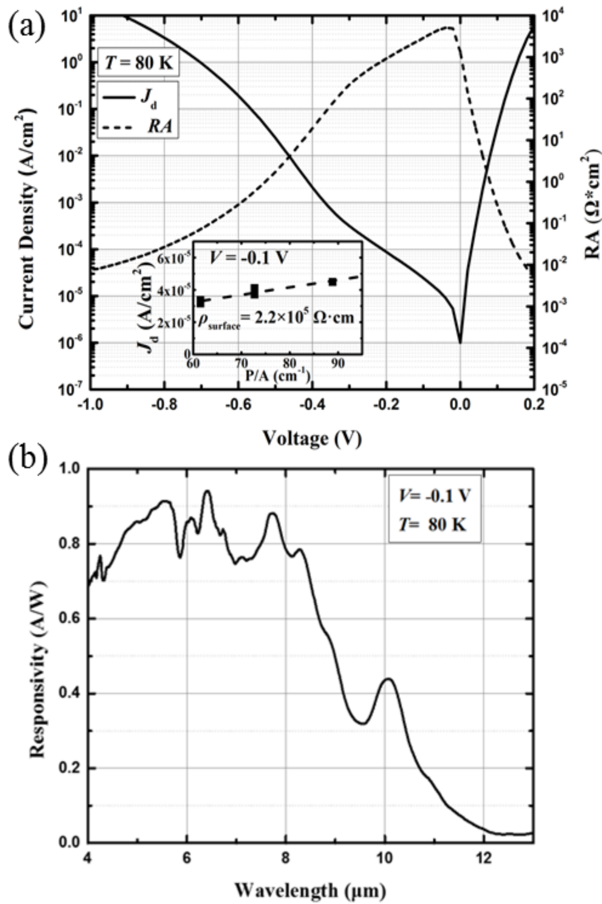

FIGURE 2. (a) Dark current density and *RA* of a single element detector. The inset is dark current density vs *P/A*. (b) Spectral responsivity of a single element detector.

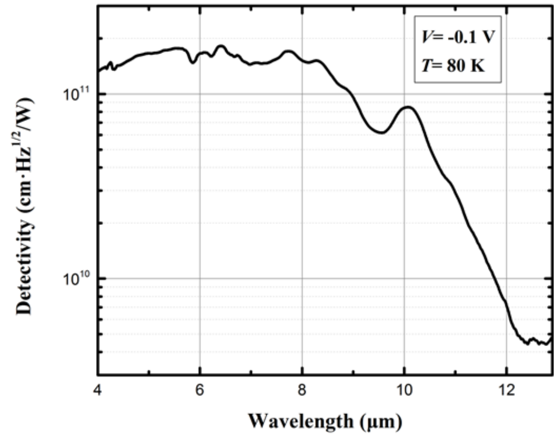

FIGURE 3. Specific detectivity of a single element detector.

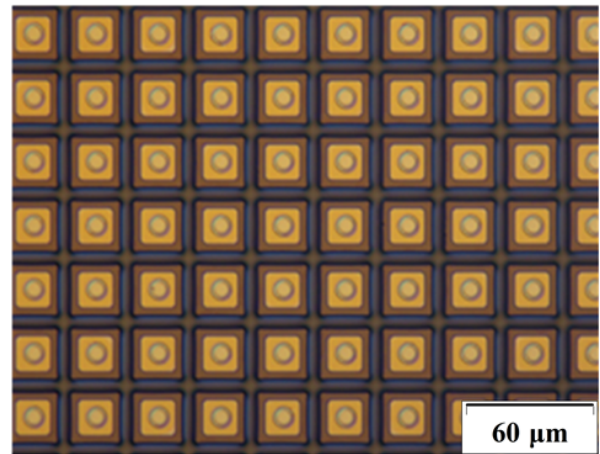

FIGURE 4. Micrograph of an array after under-bump metallization deposition.

was measured by a FTIR system, calibrated by a 600 K point-source blackbody with front side illumination. The result is shown in Fig. 2(b). At -0.1 V and 80 K, the device exhibits a 50% cut-off wavelength at 10.1 μm and 100% cut-off wavelength at 12 μm. The responsivity reaches the peak of 0.88 A/W and A/W at 7.7 μm, corresponding to a quantum efficiency of 14.2%. At 10 μm, the QE is 5.5%. The dip around 8∼9 μm was identified as a signature absorption of SiO_2 passivation layer. The cut-off in Fig. 2(b) is not steep due to the use of a thin absorber. Fig. 3 plots the specific detectivity (D^*_λ) spectrum, which is given by:

$$D^*_\lambda = R_\lambda(2qJ_d + \frac{4k_BT}{RA})^{-\frac{1}{2}} \tag{2}$$

In Eq. (2), q is the electronic charge, k_B is Boltzmann's constant, and T is the temperature. At −0.1 V and 80 K, the device achieves a peak detectivity ($D^*_{\lambda p}$) of 1.7×10^{11} cm·$Hz^{1/2}$/W at 7.7 μm, which is comparable to those reported for MBE-grown detectors with similar cut-off wavelengths [4], [21], [22].

IV. MOCVD-GROWN InAs/GaSb SUPERLATTICE FOCAL PLANE ARRAYS

For FPA fabrication, the wafer was first etched using an ICP dry etching system. The 320 × 256 arrays consisted of 25 × 25 μm^2 mesas with a pitch of 30 × 30 μm^2. Top and bottom metal contacts were formed by depositing Ti (25 nm)/Pt (55 nm)/Au (300 nm). The devices were passivated by PECVD-grown SiO_2. Windows were opened in the passivation layer using RIE. Ti (25 nm)/Au (300 nm) was then deposited as an under-bump metallization layer, as shown in Fig. 4. Then, 8 μm tall indium bumps were deposited on both the arrays and the read out integrated circuit (ROIC), which is the ISC9705 from Indigo Systems. The FPAs were then hybridized to the ROIC at room temperature. In order to improve the mechanical reliability of the arrays, the FPAs were underfilled with low viscosity epoxy. Finally, because the absorption of LWIR from the InAs substrate is low enough to perform imaging, the substrate was only polished to reduce the diffuse reflection of incident infrared radiation without thinning down. It should be noted that no antireflection coating was applied.

After processing, the 320 × 256 LWIR FPA was mounted in a leadless ceramic chip carrier (LCCC) and loaded into an infrared detector dewar. With an integration time of 1.9 ms and a lens F-number of 2.0, the signal level, the noise level,

FIGURE 5. Image taken by the MOCVD-grown LWIR T2SL FPA camera with an integration time of 1.9 ms.

the noise equivalent temperature difference (NETD) and the operability were measured at 80 K. NETD of the FPA can be calculated using the following formula [23]:

$$\mathrm{NETD} = \frac{T_{high} - T_{low}}{V_S / V_N} \tag{3}$$

where V_S is the output voltage, the V_N is the noise voltage, T_{high} is the high temperature and T_{low} is the low temperature. The temperatures of 293 K and 308 K were utilized as the low and high plane-source blackbody temperature in measurement. At -0.1 V and 80 K, the average NETD was determined as 51.1 mK. In the test, the operable pixels are defined as the pixels having a responsivity greater than half of the average responsivity and a noise voltage lower than twice the average noise voltage. The non-uniformity is defined as the ratio of root mean square deviation of responsivity and average responsivity of each operable pixel. The operability and the non-uniformity were then measured as 96.96% and 4.97%, respectively. The non-operable pixels are due to the use of thick substrate, which increases the thermal stress caused by the different thermal expansion of the InAs substrate and the silicon ROIC. The non-uniformity is caused by material defects and unoptimized fabrication process. The detectivity of the FPA was calculated using the following formula:

$$D^*_{\mathrm{bb}} = \frac{V_S * (4F^2 + 1)}{\alpha V_N (T^4_{high} - T^4_{low})\sqrt{2\pi A}} \tag{4}$$

$$D^*_{\lambda p} = D^*_{bb} * G \tag{5}$$

where $D_{\mathrm{bb}}{}^*$ is the average blackbody detectivity, F is the F-number of the lens, α is the Stefan-Boltzmann constant, τ is the integral time and G is the G-factor obtained from relative spectral response. With a 1.9 ms integration time, $D_{\mathrm{bb}}{}^*$ and the mean responsivity reached 7.1×10^9 cm·Hz$^{1/2}$/W and 1.0×10^8 V/W, respectively. G was calibrated as 6.7 and $D^*_{\lambda p}$ was calculated to be 2.3×10^{10} cm·Hz$^{1/2}$/W. Compared to the single element detector, the lower $D_{\lambda p}{}^*$ of FPA is due to the increased surface leakage from the unoptimized fabrication process and the absorption from the InAs substrate. At an operating temperature of 80 K, an image was taken by the FPA camera with 300 K background without two-point non-uniformity correction, as shown in Fig. 5. A clear image was obtained by this MOCVD-grown LWIR FPA. Although the performance of the FPA is still inferior to those of the state-of-art MBE-grown FPAs, it definitely demonstrates the potential of MOCVD-grown T2SL materials for high-quality imaging. Further improvement of the FPA performance, such as higher operability and higher detectivity, is expected by optimizing the fabrication process, thinning down the InAs substrate, and applying the antireflection coating.

V. CONCLUSION

In conclusion, we have demonstrated MOCVD-grown LWIR T2SL single detectors and FPAs. At 80 K and a bias voltage of −0.1 V, a single element detector exhibited a 50% cut-off wavelength of 10.1 μm, a dark current density of 2.5×10^{-5} A/cm^2, a peak responsivity of 0.88 A/W and a peak detectivity of 1.7×10^{11} cm·Hz$^{1/2}$/W. For a 320×256 FPA, the NETD was measured as 51.1 mK with a 1.9 ms integration time, and the peak detectivity reached 2.3×10^{10} cm·Hz$^{1/2}$/W without antireflection coating. The operability and non-uniformity were 96.96% and 4.97%, respectively. Clear image was taken by the FPA camera. To the best of our knowledge, this is the first MOCVD-grown T2SL FPA that is able to image. The FPA performance can be further improved by optimizing the fabrication process.

REFERENCES

[1] C. H. Grein, P. M. Young, M. E. Flatté, and H. Ehrenreich, "Long wavelength InAs/InGaSb infrared detectors: Optimization of carrier lifetimes," *J. Appl. Phys.*, vol. 78, no. 12, pp. 7143–7152, Dec. 1995, doi: 10.1063/1.360422.

[2] B.-M. Nguyen, G. Chen, M.-A. Hoang, and M. Razeghi, "Growth and characterization of long-wavelength infrared type-II superlattice photodiodes on a 3-in GaSb wafer," *IEEE J. Quantum Electron.*, vol. 47, no. 5, pp. 686–690, May 2011, doi: 10.1109/JQE.2010.2103049.

[3] J. M. Fastenau, D. Lubyshev, Y. Qiu, A. W. K. Liu, E. J. Koerperick, J. T. Olesberg, and D. Norton, "Sb-based IR photodetector epiwafers on 100 mm GaSb substrates manufactured by MBE," *Infr. Phys. Technol.*, vol. 59, pp. 158–162, Jul. 2013, doi: 10.1016/j.infrared.2012.12.033.

[4] P.-Y. Delaunay, B. M. Nguyen, D. Hoffman, E. K.-W. Huang, and M. Razeghi, "Background limited performance of long wavelength infrared focal plane arrays fabricated from M-structure InAs–GaSb superlattices," *IEEE J. Quantum Electron.*, vol. 45, no. 2, pp. 157–162, Feb. 2009, doi: 10.1109/JQE.2008.2002667.

[5] A. Haddadi, S. Ramezani-Darvish, G. Chen, A. M. Hoang, B.-M. Nguyen, and M. Razeghi, "High operability 1024 × 1024 long wavelength type-II superlattice focal plane array," *IEEE J. Quantum Electron.*, vol. 48, no. 2, pp. 221–228, Feb. 2012, doi: 10.1109/JQE.2011.2175903.

[6] S. D. Gunapala *et al.*, "Demonstration of a 1024 × 1024 pixel InAs-GaSb superlattice focal plane array," *IEEE Photon. Technol. Lett.*, vol. 22, no. 24, pp. 1856–1858, Dec. 2010, doi: 10.1109/LPT.2010.2089677.

[7] S. B. Rafol, A. Soibel, A. Khoshakhlagh, J. Nguyen, J. K. Liu, J. M. Mumolo, S. A. Keo, L. Hoglund, D. Z. Ting, and S. D. Gunapala, "Performance of a 1/4 VGA format long-wavelength infrared antimonides-based superlattice focal plane array," *IEEE J. Quantum Electron.*, vol. 48, no. 7, pp. 878–884, Jul. 2012, doi: 10.1109/JQE.2012.2193557.

[8] R. Rehm, M. Walther, J. Schmitz, F. Rutz, J. Fleißner, R. Scheibner, and J. Ziegler, "InAs/GaSb superlattices for advanced infrared focal plane arrays," *Infr. Phys. Technol.*, vol. 52, no. 6, pp. 344–347, Nov. 2009, doi: 10.1016/j.infrared.2009.09.005.

[9] L. Höglund, C. Asplund, R. M. von Würtemberg, H. Kataria, A. Gamfeldt, S. Smuk, H. Martijn, and E. Costard, "Manufacturability of type-II InAs/GaSb superlattice detectors for infrared imaging," *Infr. Phys. Technol.*, vol. 84, pp. 28–32, Aug. 2017, doi: 10.1016/j.infrared.2017.03.002.

[10] P.-Y. Delaunay, B. M. Nguyen, D. Hoffman, and M. Razeghi, "High-performance focal plane array based on InAs–GaSb superlattices with a 10-μm cutoff wavelength," *IEEE J. Quantum Electron.*, vol. 44, no. 5, pp. 462–467, May 2008, doi: 10.1109/JQE.2008.916701.

[11] D. H. Wu, A. Dehzangi, Y. Y. Zhang, and M. Razeghi, "Demonstration of long wavelength infrared type-II InAs/$InAs_{1-x}Sb_x$ superlattices photodiodes on GaSb substrate grown by metalorganic chemical vapor deposition," *Appl. Phys. Lett.*, vol. 112, no. 24, Jun. 2018, Art. no. 241103, doi: 10.1063/1.5035308.

[12] Y. Huang, M. Xiong, Q. Wu, X. Dong, Y. Zhao, Y. Zhao, W. Shi, X. Miao, and B. Zhang, "High-performance mid-wavelength InAs/GaSb superlattice infrared detectors grown by production-scale metalorganic chemical vapor deposition," *IEEE J. Quantum Electron.*, vol. 53, no. 5, Oct. 2017, Art. no. 4000305, doi: 10.1109/JQE.2017.2740121.

[13] X. Li, Y. Zhao, M. Xiong, Q.-H. Wu, Y. Teng, X.-J. Hao, Y. Huang, S.-Y. Hu, and X. Zhu, "High-quality InSb grown on semi-insulting GaAs substrates by metalorganic chemical vapor deposition for Hall sensor application," *Chin. Phys. Lett.*, vol. 36, no. 1, Jan. 2019, Art. no. 017302, doi: 10.1088/0256-307X/36/1/017302.

[14] X. Li, Y. Zhao, Q. Wu, Y. Teng, X. Hao, and Y. Huang, "Exploring the optimum growth conditions for InAs/GaSb and GaAs/GaSb superlattices on InAs substrates by metalorganic chemical vapor deposition," *J. Cryst. Growth*, vol. 502, pp. 71–75, Nov. 2018, doi: 10.1016/j.jcrysgro.2018.09.003.

[15] X. Li, J. Cui, Y. Zhao, Q. Wu, Y. Teng, X. Hao, Y. Chen, J. Liu, H. Zhu, Y. Huang, and Y. Yao, "Characterization of InAs/GaSb superlattices grown by MOCVD with atomic resolution," *J. Appl. Phys.*, vol. 127, no. 4, Jan. 2020, Art. no. 045305, doi: 10.1063/1.5115269.

[16] Y. Teng, Y. Zhao, Q. Wu, X. Li, X. Hao, M. Xiong, and Y. Huang, "High-performance long-wavelength InAs/GaSb superlattice detectors grown by MOCVD," *IEEE Photon. Technol. Lett.*, vol. 31, no. 2, pp. 185–188, Jan. 15, 2019, doi: 10.1109/LPT.2018.2889575.

[17] Y. Zhao, Y. Teng, X. Hao, Q. Wu, J. Miao, X. Li, M. Xiong, and Y. Huang, "Optimization of long-wavelength InAs/GaSb superlattice photodiodes with al-free Barriers," *IEEE Photon. Technol. Lett.*, vol. 32, no. 1, pp. 19–22, Jan. 1, 2020, doi: 10.1109/LPT.2019.2955562.

[18] X. Hao, Z. Deng, J. Huang, Y. Huang, H. Yang, Y. Teng, Y. Zhao, Q. Wu, X. Li, J. Liu, Y. Chen, H. Zhu, and B. Chen, "Demonstration of a dual-band InAs/GaSb type-II superlattice infrared detector based on a single heterojunction diode," *IEEE J. Quantum Electron.*, vol. 56, no. 2, Apr. 2020, Art. no. 4300106, doi: 10.1109/JQE.2019.2961123.

[19] E. K.-W. Huang, D. Hoffman, B.-M. Nguyen, P.-Y. Delaunay, and M. Razeghi, "Surface leakage reduction in narrow band gap type-II antimonide-based superlattice photodiodes," *Appl. Phys. Lett.*, vol. 94, no. 5, Feb. 2009, Art. no. 053506, doi: 10.1063/1.3078282.

[20] N. C. Henry, A. Brown, D. B. Knorr, N. Baril, E. Nallon, J. L. Lenhart, M. Tidrow, and S. Bandara, "Surface conductivity of InAs/GaSb superlattice infrared detectors treated with thiolated self assembled monolayers," *Appl. Phys. Lett.*, vol. 108, no. 1, Jan. 2016, Art. no. 011606, doi: 10.1063/1.4938168.

[21] N. Gautam, S. Myers, A. V. Barve, B. Klein, E. P. Smith, D. R. Rhiger, H. S. Kim, Z.-B. Tian, and S. Krishna, "Barrier engineered infrared photodetectors based on type-II InAs/GaSb strained layer superlattices," *IEEE J. Quantum Electron.*, vol. 49, no. 2, pp. 211–217, Feb. 2013, doi: 10.1109/JQE.2012.2236643.

[22] A. Haddadi, G. Chen, R. Chevallier, A. M. Hoang, and M. Razeghi, "InAs/$InAs_{1-x}Sb_x$ type-II superlattices for high performance long wavelength infrared detection," *Appl. Phys. Lett.*, vol. 105, no. 12, Sep. 2014, Art. no. 121104, doi: 10.1063/1.4896271.

[23] P.-Y. Delaunay, B. M. Nguyen, D. Hoffman, and M. Razeghi, "320×256 infrared focal plane array based on type-II InAs/GaSb superlattice with a 12-μm cutoff wavelength," *Proc. SPIE*, vol. 6542, May 2007, Art. no. 654204, doi: 10.1117/12.723832.

YAN TENG was born in Anhui, China. He received the B.S. degree from the College of Materials Science and Engineering, Nanjing Tech University, in 2012. He is currently pursuing the Ph.D. degree with the University of Science and Technology of China. His current research interests include photonic and electronic devices, and device processing based on III-V compound semiconductors.

XIUJUN HAO was born in Hebei, China. He received the B.S. degree from the Suzhou University of Science and Technology, in 2014. He is currently pursuing the Ph.D. degree with the School of Physical Science and Technology, ShanghaiTech University, China. His major is materials science and engineering. His research interest includes devices and nanostructures based on III–V compound semiconductors.

HONG ZHU was born in Anhui, China. She received the B.S. degree in polymer materials and engineering from Anhui Polytechnic University, in 2018. She is currently pursuing the Ph.D. degree with the University of Science and Technology of China. Her current research interest includes metal-organic chemical vapor deposition based on III-V compound semiconductors.

HE ZHU was born in Shandong, China. He received the B.E. degree from the Hubei University of Technology, in 2017. He is currently pursuing the Ph.D. degree with the University of Science and Technology of China. His current research interests include photonic and electronic devices, and device processing based on III-V compound semiconductors.

JIAFENG LIU was born in Anhui, China. He received the B.S. degree in inorganic non-metallic materials engineering from Hefei University, in 2017. He is currently pursuing the M.S. degree in materials engineering with the University of Science and Technology of China, Hefei, China. His current research interest includes photonic and electronic device and processing based on III-V compound semiconductors.

YUNLONG HUAI was born in Anhui, China. He received the B.S. degree in lamps and lighting from the Anhui University of Technology, in 2019. He is currently pursuing the master's degree with the University of Science and Technology of China. His current research interests include photonic and electronic device and processing based on III-V compound semiconductors.

MENG LI was born in Jangsu, China. She received the B.S. degree in chemistry from the Suzhou University of Science and Technology, in 2019. She is currently a Graduate Student in materials and science with ShanghaiTech University. Her main research interests include electrical properties and structural characterization of III-V compound semiconductors.

MING LIU was born in Jiangxi, China. He received the B.S. degree from Harbin Engineering University, in 2006, and the M.S. degree in physical electronics from the North China Research Institute of Electro-Optics, Beijing, China, in 2009. He is currently a Senior Process Engineer at CETC Electro-Optics Technology Corporation Ltd. His current research interests include photonic and electronic materials, devices, and infrared focal plane arrays processing based on III-V and II-VI compound semiconductors.

WEIRONG XING was born in Hebei, China. He received the B.S. degree in materials science and engineering from Northwestern Polytechnical University, in 2010, and the M.S. degree in physical electronics from the North China Research Institute of Electro-Optics, Beijing, China, in 2013. He is currently a Senior Process Engineer at CETC Electro-Optics Technology Corporation Ltd. His current research interests include photonic and electronic materials, devices, and infrared focal plane arrays processing.

BAILE CHEN (Senior Member, IEEE) received the bachelor's degree in physics from the Department of Modern Physics, University of Science and Technology of China, Hefei, China, in 2007, and the master's degree in physics and the Ph.D. degree in electrical engineering from the University of Virginia, Charlottesville, VA, USA, in 2009 and 2013, respectively. In February 2013, he joined at Qorvo Inc., OR, USA, as a RF Product Development Engineer working on various RF power amplifiers and BAW filters for RF wireless communication systems. In January 2016, he joined the School of Information Science and Technology, ShanghaiTech University, as a Tenure Track Assistant Professor and a PI. His research interests include III-V compound semiconductor materials and devices and silicon photonics.

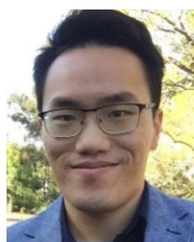

ZHUO DENG received the B.S. and Ph.D. degrees from The University of Hong Kong, Hong Kong, in 2010 and 2015, respectively. In 2015, he worked as a Research Associate with the Department of Physics, The University of Hong Kong, where he has been engaged in research of multijunction photovoltaics based on III–V compound semiconductors. In 2016, he joined the School of Information Science and Technology, ShanghaiTech University, as a Research Fellow. His current research interests include design, fabrication, and characterization of infrared photodetectors based on III–V compound semiconductor nanostructures.

YONG HUANG was born in Chongqing, China. He received the B.S. degree in materials science and engineering from Tsinghua University, in 2002, and the M.S. degree in electronics and optoelectronics from the Institute of Semiconductors, Chinese Academy of Sciences, Beijing, China, in 2005, and the Ph.D. degree in electrical and computer engineering from the Georgia Institute of Technology, Atlanta, in 2010. He worked at IQE Inc., Taunton, MA, USA, as a Senior Process Engineer, from 2011 to 2014. He is currently a Professor with the Suzhou Institute of Nano-Tech and Nano-Bionics, Chinese Academy of Sciences. His current research interests include photonic and electronic materials, devices, and nanostructures based on III-V compound semiconductors.